tions, and reversely, the suppression of G2A internalization is relieved when the pH value is above 7.

## MATERIALS AND METHODS

### Reagents

Lysophosphatidylcholine (LPC, 18:0) was purchased from Avanti Polar Lipids (Alabaster, AL, USA). Alexa Fluor 488 carboxylic acid, succinimidyl ester, mixed isomers (AF488-NHS), Alexa Fluor 647 (AF647)-labeled human transferrin, and LysoTraker Red DND-99 were from Invitrogen (Carlsbad, CA, USA). The anti-HA antibody FITC conjugate was purchased from Bethyl Laboratories (Montgomery, TX, USA).

### Preparation of SrtA and the AF488-conjugated LPETGG peptide

SrtA from *S. aureus* was expressed and purified by following our previous report (37). A hexapeptide LPETGG was prepared by standard Fmoc solid-phase peptide synthesis and purified by reversed-phase high-performance liquid chromatography (RP-HPLC). The N terminus of the LPETGG peptide was modified with AF488-NHS in dry dimethyl sulfoxide including excess diisopropylethylamine. The product, AF488-modified LPETGG peptide (AF488-LPETGG), was purified by RP-HPLC and identified with matrix-assisted laser desorption and ionization time-of-flight mass spectrometry, as previously reported (38).

### Preparation of expression plasmids

The expression plasmid for $LPETG_5$-G2A was constructed as follows. The gene encoding human G2A was subcloned into *Eco*RI and *Kpn*I sites of the pCXN2.1-HA vector, as previously reported (24), and was designated as pCXN2.1-HA-G2A. The gene encoding the LPETGGGGG sequence was inserted into pCXN2.1-HA-G2A by PCR using the forward primer (5′-AAAACTCGAGGCCATGCTACCCGAGACTGGTGGCGGAGGTGGCTACCCCTACGACGTGCCCGAC-3′) and the reverse primer (5′-AAAAGAATTCAGCAGGACTCCTCAATCAGCCTC-3′) to yield pCXN2.1-$LPETG_5$-HA-G2A. The expression plasmid for $mRFP\text{-}NLS_3$, pcDNA-mRFP-NLS, was constructed as presented in previous work (37).

### Cell culture and transfection

Human embryonic kidney (HEK) 293T cells were cultured in Dulbecco's modified Eagle's medium (DMEM) supplemented with 10% fetal bovine serum (Gibco Invitrogen, San Diego, CA, USA), 0.584 g/L glutamine, 10% $NaHCO_3$ and kanamycin on a poly L-lysine-coated 35 mm glass-base dish (Iwaki Glass, Iwaki City, Japan) at 37°C with 0.5% $CO_2$ for 24 h before transfection. HEK293T cells were then cotransfected with pCXN2.1-$LPETG_5$-HA-G2A and pcDNA-mRFP-NLS using the Lipofectamine Plus reagent (Invitrogen), according to the manufacturer's protocol. Before the labeling experiments, the transfected HEK293T cells were cultured for 24 h in the $CO_2$ incubator where the temperature and the $CO_2$ concentration were set at 37°C and 0.5% $CO_2$, respectively.

### Preparation of culture media with acidic and neutral pHs

The culture media with pH values of 6.5 and 7.7 were prepared by 50-fold dilution of 1 M HEM buffer, a HEPES/EPPS/MES mixture (each 333 mM), with the pH value of 6.0 and 8.4 in DMEM containing 0.5 g/L $NaHCO_3$, and 0.1% bovine serum albumin (BSA) [DMEM (0.1% BSA)], respectively. These media were denoted as DMEM (20 mM HEM, 0.1% BSA) (pH 6.5 or 7.7).

### SrtA-mediated labeling of G2A on cell surfaces

The culture medium was removed from the dishes, and the cotransfected HEK293T cells were washed once with 1 ml of DMEM(–) (0.1% BSA). The cells were then incubated in a DMEM (0.1% BSA) containing 5 μM LPC (18:0) for 2 h in the $CO_2$ incubator. After removal of the medium, the cells were incubated in DMEM (0.1% BSA) containing 1 mM triglycine, 30 μM SrtA, and 0 or 5 μM LPC(18:0) at 37°C for 30 min for cleavage. The cells were subsequently incubated in DMEM (0.1% BSA) containing 30 μM SrtA, 10 μM AF488-LPETGG, and 0 or 5 μM LPC(18:0) at 37°C for 15 min for labeling. After labeling, the cells were washed with 1 ml DMEM (–) (0.1% BSA) three times and subjected to confocal microscopy.

### Confocal microscopy observations of SrtA-mediated labeled G2A

The images of labeled cells were obtained using an LSM510 laser scanning confocal microscope (Carl Zeiss, Jena, Germany) with a ×40 objective lens. Time-lapse observation of the labeled G2A was performed by incubating the cells in DMEM (20 mM HEM, 0.1% BSA) (pH 6.5 or 7.7) on the stage of the microscope with a XL-Clear S1 incubator system (from Carl Zeiss, Jena, Germany). In the pH jump experiments, the pH of the medium was instantly increased from 6.5 to 8.5 by adding a small amount of 10% $NaHCO_3$ aqueous solution into DMEM (20 mM HEM, 0.1% BSA) (pH 6.5) in the dish, and then, reacidification to pH 6.5 was achieved by subsequently adding a small amount of an HCl solution.

### Fluorescent staining with intracellular markers

For staining endosomal vesicles or late endosomes/lysosomes, the SrtA-mediated labeled cells were incubated in DMEM (20 mM HEM, 0.1% BSA) containing 10 μg/ml AF647-labeled transferrin, or 100 nM LysoTracker Red DND-99, respectively. After incubation at 37°C for 45 min, the cells were washed with 1 ml DMEM (20 mM HEM, 0.1%BSA) three times and subjected to confocal microscopy.

### Image analysis

The images obtained, as described above, were analyzed as follows. We manually cut out the fluorescent image of a target cell along the cell membrane contour from the original image and converted this image to a grayscale image (200×200 pix). The binarized images were obtained from single-cell images by using the adaptive threshold, which was calculated from the mean brightness at each square block (45×45 pix) by the OpenCV adaptive threshold function (http://opencv.jp/opencv-2.1/cpp/miscellaneous_image_transformations.html). From the binarized images, the two bunches of pixels at the cell surface and the intracellular regions were converted to the mask images with connected component labeling software (the labeling.h. function; http://oshiro.bpe.es.osaka-u.ac.jp/people/staff/imura/products/labeling/source/Labeling.h). The average brightness of each region was calculated by dividing the sum of the original pixel brightness value in the mask region with the region area. To cancel out the influence of photobleaching

and the slight pH sensitivity of the fluorescent dye, the average brightness of each region was normalized with the total average brightness of two regions, and normalized brightness of each region was plotted against the observation time of the analyzed image.

### Model fitting

To derive an analytical fitting model for pH-responsive G2A distribution, we formulated a simple model where fluorescently labeled G2A was distributed at the cell surface membrane and the intracellular domain. In addition, we made the following assumptions for this model: Only the deprotonated G2A receptor can be internalized; the G2A receptor concentrations in each compartment (cell membrane and interior) are spatially uniform; the measured fluorescence intensity is proportional to the concentration of the labeled G2A receptor; the time change of interior volume ($V_i(t)$) can be evaluated by the measurement of the interior area, as determined by fluorescence image analysis; the time change of membrane volume ($V_m(t)$) is negligible, because the size of the cells and their membrane areas determined by the fluorescence image analysis were almost constant.

The pH-dependent internalization rate of the labeled deprotonated G2A receptor can be formulated as follows. The labeled protonated G2A receptor ($G2A_{mem,de}$-$H^+$) deprotonates into a labeled deprotonated G2A ($G2A_{mem,de}$) and proton. This process can be represented schematically as follows:

$$G2A_{mem,de}\text{-}H^+ \leftrightarrow G2A_{mem,de} + H^+$$

For this dissociation process, the acid dissociation constant ($K_a$) can be defined as follows:

$$K_a = \frac{[G2A_{mem,de}][H^+]}{[G2A_{mem,de}\text{-}H^+]}$$

Here, $[G2A_{mem,de}] + [G2A_{mem,de}\text{-}H^+]$ is the concentration of the total labeled G2A receptor on the cell membrane ($[G2A_{mem}]$).

$$[G2A_{mem}] = [G2A_{mem,de}] + [G2A_{mem,de}\text{-}H^+]$$

The concentration of labeled deprotonated G2A receptor ($[G2A_{mem,de}]$) can be shown as follows:

$$[G2A_{mem,de}] = \frac{K_a}{K_a + [H^+]}[G2A_{mem}]$$

We assumed that only the deprotonated G2A receptor internalizes into the interior compartment and that the internalization rate of the labeled G2A receptor is proportional to the concentration of labeled deprotonated G2A receptor on the cell membrane ($[G2A_{mem,de}]$):

$$G2A_{mem,de} \xrightarrow{k_i} G2A_{int}$$

Thus, the internalization rate can be shown as below:

$$\text{Internalize rate} = k_i[G2A_{mem,de}] = k_i\frac{K_a}{K_a + [H^+]}[G2A_{mem}]$$

The changes in the labeled G2A receptor concentration at the membrane and within the interior compartments can be shown by the following mass balance equations:

$$\frac{d[G2A_{mem}]}{dt} = k_r[G2A_{int}]\frac{V_i(t)}{V_m} - k_i\frac{K_a}{K_a + [H^+]}[G2A_{mem}]$$

$$\frac{d[G2A_{int}]}{dt} = -k_r[G2A_{int}] + k_i\frac{K_a}{K_a + [H^+]}[G2A_{mem}]\frac{V_m}{V_i(t)} + \frac{[G2A_{int}]}{V_i(t)}\frac{dV_i(t)}{dt}$$

Here,

$t < 900$; pH = 8.5, $[H^+] = 1 \times 10^{-8.5}$

$t \geq 900$; pH = 6.5, $[H^+] = 1 \times 10^{-6.5}$

Furthermore, the relative volume of $V_i(t)$ to $V_m$ was obtained by image analysis as shown in the supporting information (Supplemental Figs. S1 and S2 and Supplemental Table S1).

The simulation was carried out in the Vcell platform. The values of $k_r$ and $k_i$ were searched by the 2D parameter scan ((10×10 samples) × 2 sets) at each p*Ka* value (6.5, 7.0, 7.5 and 8.0), and the best-fitted ones were determined by minimizing the root-mean-square (RMS) error between the normalized measured fluorescence intensity and the simulated labeled G2A receptor concentration calculated by the Excel 2010 software (Microsoft, Redmond, WA, USA; Supplemental Fig. S3 and Supplemental Table S2).

## RESULTS

### Sortase-mediated labeling of G2A on cell surfaces

The N terminus of tag-fused G2A can be labeled with a fluorescent labeling reagent using our previously reported method based on a 2-step SrtA-catalyzed reaction on cell surfaces (Fig. 1) (39, 40). In the first step, to expose the N-terminal pentaglycine sequence on the tag-fused G2A, the LPETGGGGG sequence of the tag was site-specifically cleaved between threonine and glycine by treatment of G2A-expressing HEK 293T cells with SrtA and triglycine. Successively, in the second step, the labeling reagent consisting of the AF488-conjugated LPETGG peptide was linked to the exposed N-terminal pentaglycine on G2A by treatment with a mixed solution of SrtA and the labeling reagent. In this study, HEK293T cells were selected as a model cell, because exogenous proteins can be highly expressed by standard lipofection of the expression plasmid. HEK293T cells were cotransfected with the expression plasmids encoding the genes of LPETGGGGG tag-fused human G2A ($LPETG_5$-G2A) and monomeric red fluorescence protein with a nuclear localized signal ($mRFP\text{-}NLS_3$), which was employed as a transfection reporter.

The SrtA-mediated labeling of $LPETG_5$-G2A was performed with or without LPC treatment. In our labeling method, only $LPETG_5$-G2A exposed on cell surfaces can be labeled, and therefore, the amount of surface expressed $LPETG_5$-G2A is critical for clearly visualizing the G2A trafficking. LPC treatment was reported to enhance the surface expression of both murine and human G2A-GFP fusion proteins in Swiss 3T3 cells or DO11.10 cells (34). Accordingly, before labeling, $LPETG_5$-G2A expression cells were incubated with DMEM containing 5 μM LPC for 2 h for increasing $LPETG_5$-G2A on cell surfaces. **Figure 2** shows the confocal microscopic images of $LPETG_5$-G2A express-

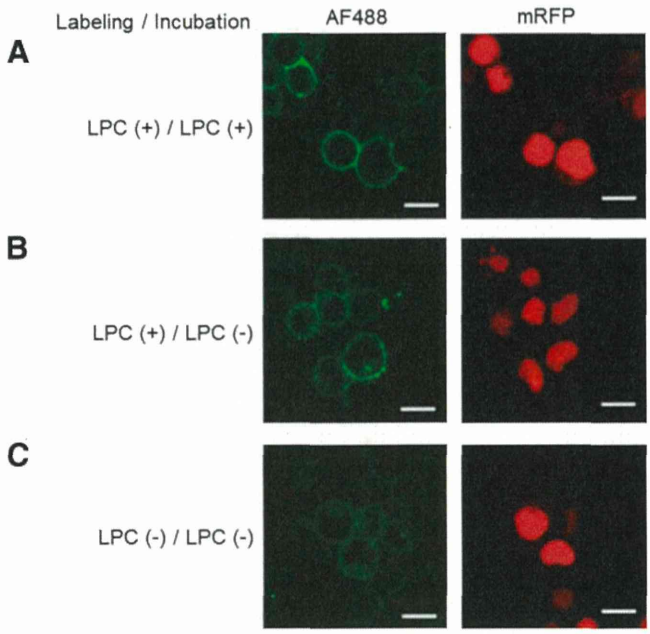


**Figure 2.** SrtA-mediated labeling of tag-fused G2A in the presence or in the absence of LPC. $LPETG_5$-G2A was labeled with an AF488-modified LPETGG peptide through the SrtA-mediated 2-step labeling method on HEK293T cells expressing mRFP-$NLS_3$ as a transfection marker in the presence (*A*, *B*) or in the absence of 5μM LPC (*C*). After removing the SrtA and the labeling reagents, the cells were successively incubated for 3 h in the presence (*A*) or in the absence of 5 μM LPC (*B*, *C*). After incubation, the green and red fluorescent images of cells were obtained with a confocal microscope. Labeling of G2A and incubation were performed in DMEM containing 0.1% BSA with or without LPC at pH 7.4. Scale bars = 20 μm.

ing cells after SrtA-mediated labeling and following incubation either in the presence or absence of 5 μM LPC. In all green fluorescent images, the fluorescence of AF488 was observed only on the transfected cells that were stained by the transfection marker protein. Accordingly, the specific labeling of $LPETG_5$-G2A on living cells was successfully confirmed under our experimental conditions with and without LPC, and AF488-labeled $LPETG_5$-G2A (AF488-G2A) was clearly visualized by confocal microscopy. In the presence of LPC during labeling (Fig. 2*A*, *B*), the green fluorescent images appeared brighter than the images taken for samples where LPC was absent (Fig. 2*C*). This result indicates that the amount of AF488-G2A was increased by LPC-induced enhancement of $LPETG_5$-G2A retention on cell surfaces during labeling.

After labeling, the fluorescence of AF488-G2A was observed in the presence or in the absence of LPC. As shown in Fig. 2*B*, a part of AF488-G2A on cell surfaces was triggered to internalize into intracellular compartments within 3 h following washout of LPC, while almost all AF488-G2A was retained on cell surfaces when 5μM LPC was present (Fig. 2*A*). This result clearly shows that LPC treatment blocked the spontaneous internalization of AF488-G2A. The blockage of AF488-G2A internalization is consistent with and complementary to the previously reported LPC-triggered surface relocation of G2A-GFP (34). In addition, it was demonstrated that the SrtA-mediated labeling with LPC treatment is useful for strictly chasing the intracellular movement of the cell-surface G2A: only the cell-surface G2A could be specifically labeled, and the labeled G2A could be retained on the cell surface until LPC was washed out at the desired time. Therefore, the present method was applied to further investigate the influence of pH on G2A trafficking.

### Extracellular pH change-induced G2A trafficking

We first examined the effect of the extracellular pH on G2A internalization from cell surfaces into intracellular compartments. In our previous report, G2A-mediated signal transduction at various pHs from 6.8 to 8.8 was evaluated by promoter-luciferase reporter assay, and the promoter activation gradually decreased as the pH value increased, resulting in slight activity at pH 8.6 (24). Accordingly, in this study, G2A trafficking was observed in this pH range. First, $LPETG_5$-G2A on the cell surface was labeled with AF488 in a medium including LPC. Next, following the washout of LPC, the time-lapsed images of AF488-G2A were obtained in a medium with pH values of 7.7 and 6.5. At pH 7.7, AF488-G2A was visualized to internalize within 40 min and to gradually accumulate in intracellular compartments over time (**Fig. 3*A***). In contrast, the intracellular accumulation of AF488-G2A was barely observed at pH 6.5, and even after incubation for 120 min a significant fraction of AF488-G2A was localized on the cell surface (Fig. 3*B*). From these results, the extracellular pH appears to influence the internalization of G2A in the absence of LPC. To strictly show the influence of the extracellular pH on G2A trafficking, the extracellular pH was instantly changed from 6.5 to 8.5 by adding a 10% $NaHCO_3$ solution into the medium during observation (**Fig. 4**). Before the pH jump, the internalization of AF488-G2A was barely observed within 35 min, as shown in Fig. 3*B*. On the other hand, AF488-G2A gradually accumulated in a certain cellular compartment within 30 min after the pH jump to 8.5 (Fig. 4, from 40 to 70 min). This change in AF488-G2A internalization on the same cells between before and after the pH jump clearly shows that the internalization of G2A was regulated by the extracellular pH: the internalization rate seems to be extremely slow under acidic pH conditions and increases when the pH is shifted to a value above neutral pH.

Next, to identify where AF488-G2A was accumulating following an increase in the extracellular pH, we examined the colocalization of AF488-G2A with two intracellular organelle markers, namely, fluorescent-labeled transferrin and LysoTracker (**Fig. 5**). The former is a marker of endosomal vesicles, and the latter stains late endosome/lysosomes. In a previous report, at neutral pH, G2A-GFP was localized on the endosomal vesicles that were stained with fluorescently labeled transferrin, whereas significant colocalization with LysoTracker, the

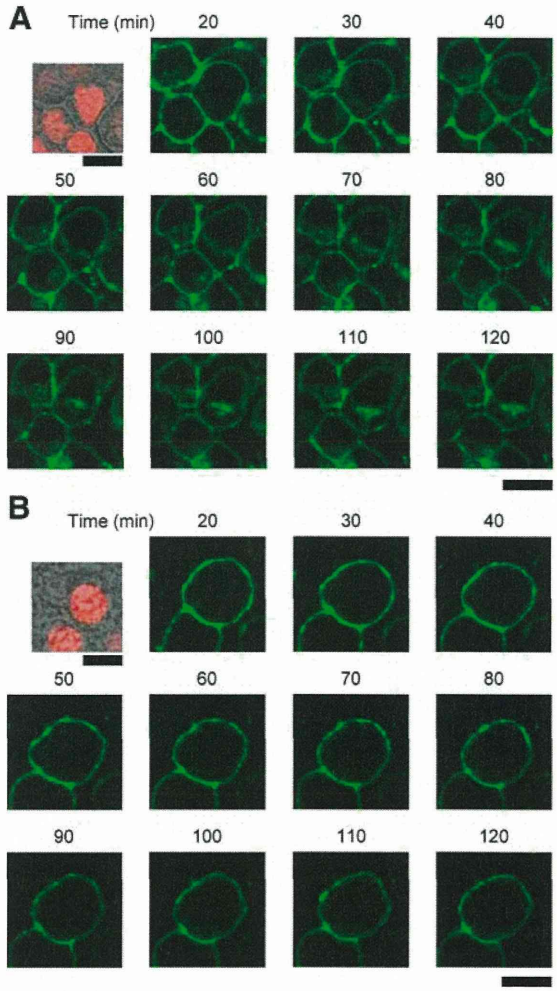


**Figure 3.** Time-course images of fluorescently labeled G2A at acidic or neutral pH values. The time-course changes in the distribution of AF488-labeled G2A in living HEK293T cells were observed at pH 7.7 (*A*) and 6.5 (*B*). The green fluorescent images of AF88-labeled G2A were obtained with a confocal microscope every 10 min, following the 20 min labeling. The red fluorescent image in the top-left corner is the image of mRFP-$NLS_3$ expressed in the transfected cells as a transfection marker. Scale bars = 20 μm.

ER marker, and the Golgi marker was not observed (34). Similarly, in this study, the AF488-G2A in the intracellular regions was found to colocalize with AF647-labeled transferrin rather than with the LysoTracker Red at pH 7.4 (Fig. 5*A*, *B*). However, at pH 6.5, almost all of the AF488-G2A was retained on cell surfaces and no colocalization with intracellular markers was observed (Fig. 5*C*, *D*). This result clearly indicates that increasing the extracellular pH to the neutral value triggers the internalization of G2A through endosomal pathways and that the internalized G2A is localized on endosomal vesicles without trafficking to the late endosome/lysosomes. Therefore, the internalized G2A is assumed to return to cellular membranes through recycling endocytosis as found for other GPCRs (31, 32).

We aimed to visualize the redistribution of AF488-G2A from endosomal vesicles to cellular membranes. After internalization of AF488-G2A at pH 8.5, the extracellular pH was shifted back to pH 6.5 by the addition of an HCl solution. If AF488-G2A returns to cell surfaces through recycling pathways, the fluorescent intensities on the cellular membranes may increase with simultaneous decrease of intracellular fluorescence. As shown in **Fig. 6*A***, the strong fluorescence of the intracellular compartments was observed to decrease immediately following the shift of the extracellular pH to an acidic value. Additionally, the cell-surface fluorescence appeared to slightly increase in parallel with the decrease of the intracellular fluorescence. To clearly show this, these time course images were analyzed by image analysis based on adaptive binarization. The analyzed data showed that the decrease in fluorescence of the cell surfaces reverted to an increase following reacidification, whereas the intracellular fluorescence was found to decrease (Fig. 6*B*, *C*). These results clearly showed that the internalized AF488-G2A was redistributed to cell surfaces by reacidification. Thus, it was first directly visualized that the G2A internalized from the cellular membrane can return to the cell surface, probably through recycling endocytosis.

To further understand the mechanism of pH change-induced distribution of G2A, we applied the two-region distribution model to fit the image analysis data. In this model, the internalization rate depends on the protonation of a key amino acid on G2A; however, the recycling rate is only proportional to the concentration of G2A in the intracellular region, independent of the extracellular pH. As shown in Fig. 6*B*, *C*, the analytical data fitted the simulated data well using this model, where the $pK_a$ value of the key amino acid on G2A was

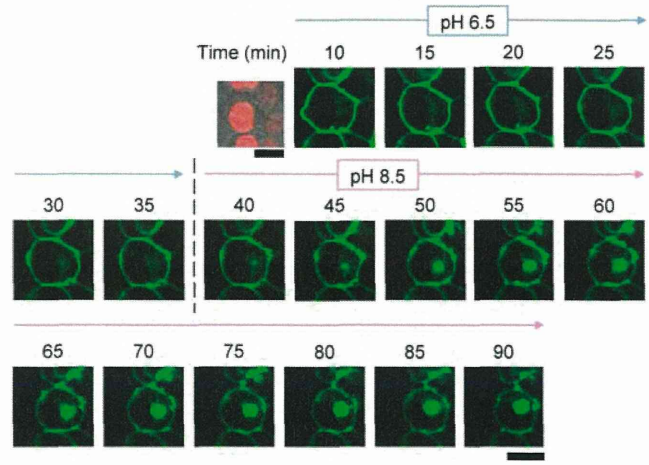


**Figure 4.** Time-course images of fluorescently labeled G2A before and after a pH jump. The time-course changes in the distribution of AF488-labeled G2A in living HEK293T cells were observed before and after a pH jump from 6.5 to 8.5. The green fluorescent images of AF488-labeled G2A were obtained with a confocal microscope every 5 min following the 10 min labeling period. At a time between 35 and 40 min after labeling, the pH value of the medium was rapidly increased on the microscope stage by the addition of a small amount of 10% $NaHCO_3$ aqueous solution. The red fluorescent image in the top-left corner is the image of mRFP-$NLS_3$ expressed in the transfected cells as a transfection marker. Scale bars = 20 μm.

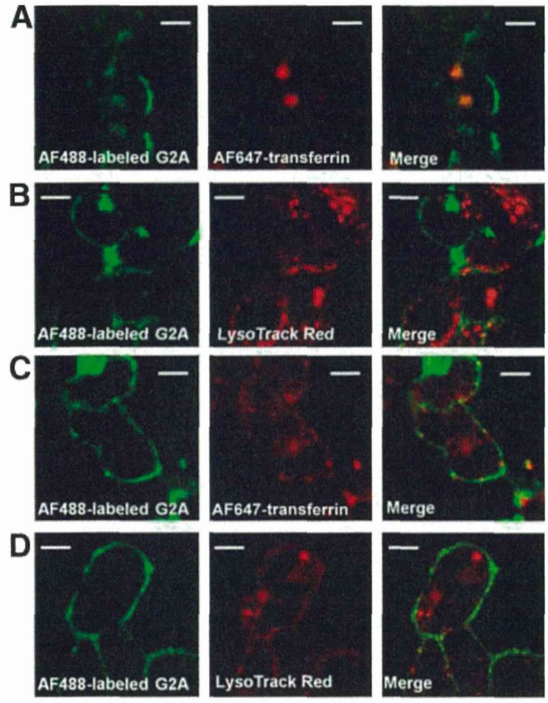


**Figure 5.** Intracellular localization of fluorescently labeled G2A at acidic or neutral pH values. The HEK293T cells dispalying AF488-labeled G2A were incuabed for 45 min in the medium containing AF647-labeled transferrin (*A*, *C*) or LysoTracker Red DND-99 (*B*, *D*). The pH of the incubation media was adjusted to 7.7 (*A*, *B*) or 6.5 (*C*, *D*). Scale bars = 10 μm.

set to 7.5 (Fig. S3). Furthermore, in this case, the internalization rate $k_i$ at pH 6.5 was one-tenth smaller than at pH 8.5 (Supplemental Table S2). Thus, the change in the internalization rate due to a shift in the extracellular pH is likely to be the main factor in inducing a change in the distribution of G2A.

## DISCUSSION

Post-translational pulse labeling enables the most accurate and simplest monitoring of protein trafficking, whereas target-specific pulse labeling with high efficiency is not easy to achieve with conventional labeling methods (35–37). In this study, the SrtA-mediated site-specific N-terminal labeling method was employed for specific pulse labeling of G2A. By using this method, highly site-specific and rapid labeling of target membrane proteins on living cells could be achieved owing to the advantages of SrtA-mediated transpeptidation, such as high substrate specificity and reactivity (39, 40). The specific labeling of G2A on living cells was successfully completed through the 2-step SrtA-mediated reaction over 45 min (Fig. 2). Furthermore, it is noteworthy that only G2A on cell surfaces was potentially labeled with the fluorescent dye. This is because both SrtA and the labeling reagent cannot spontaneously permeate the cell membrane. In addition, in this case, LPC treatment blocked the spontaneous internalization of the labeled G2A during the labeling period (Fig. 2). Accordingly, in this approach, at the beginning of the time course analysis, only the G2As that were mature and displayed on cell surfaces could be selectively visualized.

However, conventional labeling by expressing the protein as a fusion construct with a fluorescent protein clearly offers absolute specificity and certainty of targeted labeling of proteins in living cells. Since this labeling method easy to perform, this approach has been widely employed to investigate protein localization in living cells. With this approach, pulse labeling for accurately monitoring of protein dynamics requires further technology for controlling the expression timing and lifetime of the fusion proteins or using a photoactive fluorescent protein (43). For example, the pulse-chase analysis of the G2A-GFP fusion was performed by limiting the expression timing with both a tetracycline-regulated expression system and a protein synthesis inhibitor (34). In this pioneering study, G2A-GFP was expressed for 5 h just before observation. However, at the beginning of the observation, G2A-GFP at different stages in their lifetime may be observed, because G2A-GFP was continuously being synthesized, folded, modified, transported, and degraded during the period of expression. This has been previously pointed out as a disadvantage of the GFP fusion approach (43). Therefore, compared to the previous study, the present SrtA-mediated pulse-labeling method can potentially achieve a more accurate analysis of G2A trafficking.

We first visualized the pH change-dependent distribution changes of G2A in living cells by SrtA-mediated pulse labeling. Nearly a decade ago, the proton-sensitive ability of G2A was confirmed by a reporter gene assay and by measuring inositol phosphate accumulation (24). Similar to other proton-sensing GPCRs, such as OGR1 and GPR4, which are similar to G2A in structure, G2A was activated at low (*i.e.*, acidic) pH values. In this previous report, mutagenesis of His-259 of G2A led to low cell surface expression of G2A and the elimination of the low-pH-dependent activation of G2A signaling; as observed for the His-245 mutant of OGR1 (equivalent to His-259 in G2A). From these results, the relationship between the pH-dependent activation and the cell surface distribution of G2A was already a possible hypothesis. However, in the pulse-chase analysis of the G2A-GFP fusion, the pH-dependent distribution change was not observed (34). Therefore, it is necessary to reexamine the effect of pH on G2A trafficking with a more accurate monitoring method that clarifies the mechanism of the pH-dependent activation of G2A signaling.

In this study, the observed results are quite different from the results obtained using the G2A-GFP. The pH-dependent redistribution of the labeled G2A was clearly observed by microscopic time course analysis (Figs. 3, 4, and 6). This difference in the trafficking of labeled G2A is assumed to be derived from the difference of the fluorescent probes. In the present SrtA-mediated labeling, only a short fluorescent peptide

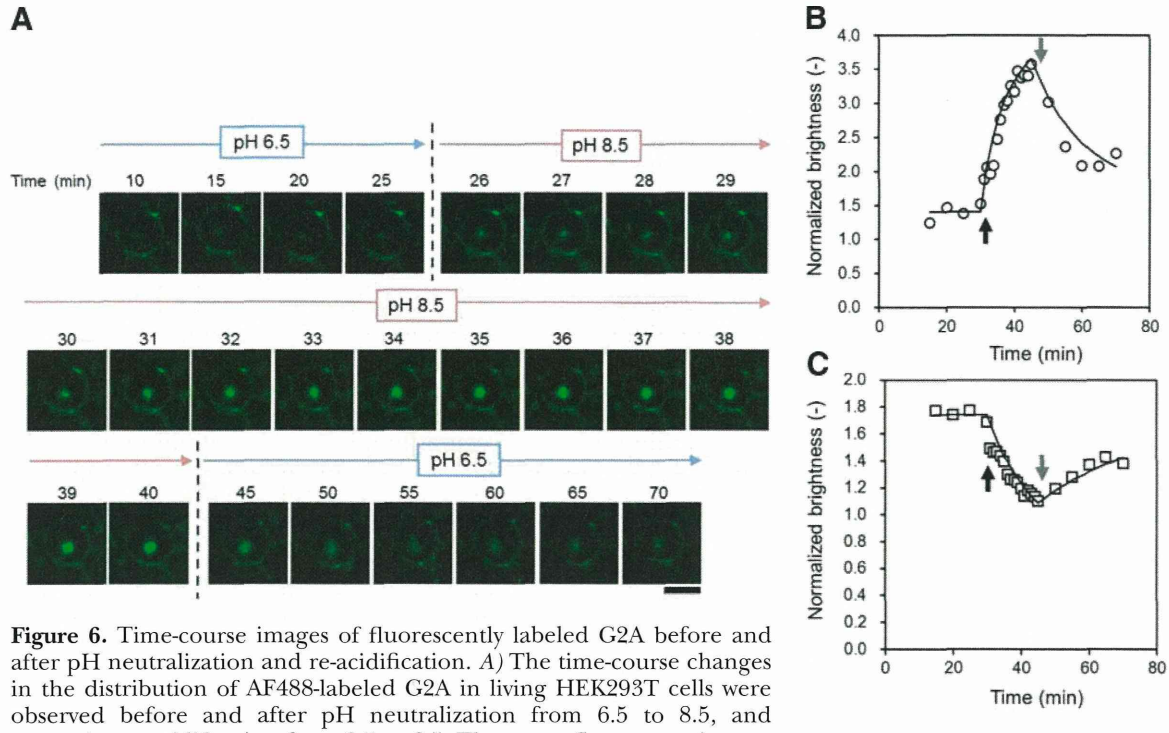


**Figure 6.** Time-course images of fluorescently labeled G2A before and after pH neutralization and re-acidification. *A)* The time-course changes in the distribution of AF488-labeled G2A in living HEK293T cells were observed before and after pH neutralization from 6.5 to 8.5, and successive re-acidification from 8.5 to 6.5. The green fluorescent images of AF488-labeled G2A were obtained with a confocal microscope every 5 min at pH 6.5 and every 1 min at pH 8.5, following the 10 min labeling period. At a time between 25 and 26 min after labeling, the pH value of the medium was rapidly increased on the microscope stage by the addition of a small amount of 10% $NaHCO_3$ aqueous solution, and at a time between 40 and 45 min, the pH was decreased by the addition of a small amount of an HCl aqueous solution. The scale bars represent 20 μm. *B)* The normalized average fluorescent brightness of the intercellular region was plotted against the time after labeling. *C)* That of the cell surface region was also plotted. The black and grey arrows indicate the timing of pH neutralizing and re-acidification, respectively. The fitting curves were obtained by stimulating a 2-region distribution model.

consisting of 9 amino acids and a small fluorescent dye was appended to the N terminus of G2A as a probe (Fig. 1), whereas a large GFP molecule was fused with G2A in the previous report (34). As a disadvantage in labeling with GFP variants as probes, it has been reported that the steric bulk of these proteins (at least 220 aa) has the potential to perturb significantly the trafficking of proteins that are fused to this marker protein (44). Furthermore, GFP is well known to be negatively charged (isoelectric point: pH 4.7–5.1) from mild acidic to neutral pH values. This negative charge of GFP might also perturb the proton-sensing molecular machinery of the GPCR subfamily, which was previously reported to consist of basic amino acid pairs such as His-17:His-84 and His-20:His-269 in OGR1 (5). Thus, we present the first pH-dependent internalization rate change of proton-sensing GPCR that has been successfully achieved using SrtA-mediated labeling with a small fluorescent probe.

GPCR is desensitized through endocytotic internalization and this process protects cells against overstimulation. Also, the intracellularly stored receptor is recycled in response to the extracellular conditions through recycling endocytosis (31, 32). Accordingly, similar to other GPCRs, the G2A distribution between the cell surface and intracellular compartments can be explained by the balance between internalization and recycling. From observation of AF488-G2A in this study, G2A internalization was first found to be blocked under an acidic pH value and relieved at pH values above 7 (Figs. 3*B* and *4*). Additionally, as shown in Fig. 6, the internalized G2A was confirmed to be returned to cell surfaces through recycling endocytosis. Based on this observation, we applied a simple 2-region distribution model to image analysis of our data. As a result, the simulation curve fitted well to the image analysis data (Fig. 6*B*, *C*). From these results, the pH-dependent G2A distribution may be explained as follows (**Fig. 7**). At an acidic pH, the G2A internalization rate is relatively slow, and most of the labeled G2A is distributed on the cell surface. Following a pH jump to pH above 7, the internalization flux of G2A surpasses the recycling flux owing to the high concentration of deprotonated G2A on the cell surface. This results in a high internalization rate of labeled G2A. Accordingly, the intracellular accumulation of labeled G2A was clearly visualized. After reacidification, the internalization rate decreased, probably owing to protonation of a key amino acid on G2A, whereas a low pH had negligible influence on the recycling rate. In addition, the concentration of labeled G2A in the intracellular region was relatively large. Accordingly, the recycling flux of labeled G2A largely surpassed the internalization flux. Thus, the low internalization rate at acidic pH values is assumed to cause

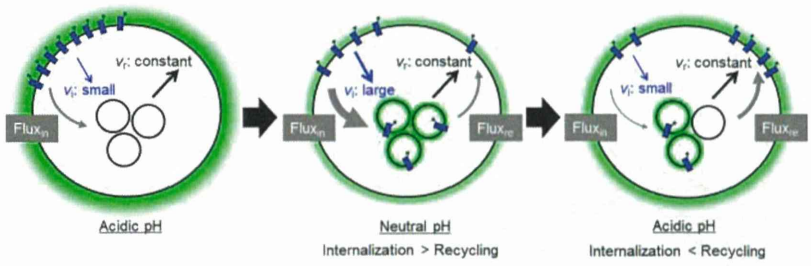


**Figure 7.** Schematic illustration showing the change in G2A localization due to the pH change-induced mechanism. At the first acidic pH after the washout of LPC, the fluorescently labeled G2A slightly internalizes owing to the small internalization rate of deprotonated G2A. After the pH jump to neutral pH, the internalization flux of the labeled G2A surpasses the recycling flux because of an increment of the internalization rate of deprotonated G2A, which is proportional to the increase of the deprotonated G2A concentration on the cell surface. After re-acidification, the recycling flux reversely overtakes the internalization flux because the internalization rate decreases again owing to the decrease in the deprotonated G2A concentration on cell surface under acidic pH conditions.

the pH change-induced redistribution of labeled G2A on the cell surface, which was observed in this study.

It was previously reported that G2A-mediated signal transduction for *zif* 268 promoter activation and IP accumulation was enhanced by lowering the extracellular pH (24). In this study, at acidic pHs, the internalization rate of G2A was drastically reduced, leading to cell surface distribution of G2A. This correlation between the signal transduction and the cell surface amount of G2A strongly suggests that protonation of G2A changes its conformation to the structure which interacts with a G protein rather than the adaptor protein for endocytosis, although the detailed endocytic machinery remains unclear. In the previous report, G2A-GFP was also reported to be constitutively internalized in the absence of LPC at neutral pHs, and addition of LPC induced surface distribution of G2A with activation of G2A signal transduction for cell migration (33). From these, both proton recognition and LPC binding may cause conformational changes, resulting in dissociation of G2A from endocytic machinery proteins. Furthermore, LPC binding was also reported to antagonize proton-induced activation of signal transduction (24). Accordingly, proton recognition and LPC binding are assumed to induce different G2A conformations which associate with different G proteins, respectively. Further experiments are needed to fully understand the mechanism of pH change-dependent G2A signal transduction. However, the present study has clearly visualized pH change-dependent G2A distribution changes, and these results should promote our understanding of the proton-sensing system of G2A and provide clues to the common mechanism by which the activities of proton-sensing GPCRs are regulated by the extracellular pH. FJ

This work was supported by a Ministry of Education, Culture, Sports, Science and Technology, Japan, Grant-in-Aid for Challenging Exploratory Research 246564498 and a grant for the Center for NanoBio Integration (CNBI). W. L. was supported by the China Scholarship Council (CSC) and the National Science Foundation of China (No. 31070742).

## REFERENCES

1. Spiegel, S., and Milstien, S. (1995) Sphingolipid metabolites: members of a new class of lipid second messengers. *J. Membr. Biol.* **146,** 225–237
2. Moolenaar, W. H. (1999) Bioactive lysophospholipids and their G protein-coupled receptors. *Exp. Cell Res.* **253,** 230–238
3. Lombardi, M. S., Kavelaars, A., and Heijnen, C. J. (2002) Role and modulation of G protein-coupled receptor signaling in inflammatory processes. *Crit. Rev. Immunol.* **22,** 141–163
4. Ghanouni, P., Schambye, H., Seifert, R., Lee, T. W., Rasmussen, S. G. F., Gether, U., and Kobilka, B. K. (2000) The effect of pH on β2 adrenoceptor function. *J. Biol. Chem.* **275,** 3121–3127
5. Ludwig, M. G., Vanek, M., Guerini, D., Gasser, J. A., Jones, C. E., Junker, U., Hofstetter, H., Wolf, R. M., and Seuwen, K. (2003) Proton-sensing G-protein-coupled receptors. *Nature* **425,** 93–98
6. Tomura, H., Wang, J. Q., Komachi, M., Damirin, A., Mogi, C., Tobo, M., Kon, J., Misawa, N., Sato, K., and Okajima, F. (2005) Prostaglandin I(2) production and cAMP accumulation in response to acidic extracellular pH through OGR1 in human aortic smooth muscle cells. *J. Biol. Chem.* **280,** 34458–34464
7. Tobo, M., Tomura, H., Mogi, C., Wang, J. Q., Liu, J. P., Komachi, M., Damirin, A., Kimura, T., Murata, N., Kurose, H., Sato, K., and Okajima, F. (2007) Previously postulated "ligand-independent" signaling of GPR4 is mediated through proton-sensing mechanisms. *Cell. Signal.* **19,** 1745–1753
8. Chen, A., Dong, L. X., Leffler, N. R., Asch, A. S., Witte, O. N., and Yang, L. V. (2011) Activation of GPR4 by acidosis increases endothelial cell adhesion through the cAMP/Epac pathway. *PLoS One* **6,** e27586
9. Gerweck, L. E., and Seetharaman, K. (1996) Cellular pH gradient in tumor versus normal tissue: potential exploitation for the treatment of cancer. *Cancer Res.* **56,** 1194–1198
10. Vaupel, P. W., Frinak, S., and Bicher, H. I. (1981) Heterogeneous oxygen partial pressure and pH distribution in C3H mouse mammary adenocarcinoma. *Cancer Res.* **41,** 2008–2013
11. Rotin, D., Robinson, B., and Tannock, I. F. (1986) Influence of hypoxia and an acidic environment on the metabolism and viability of cultured cells: potential implications for cell death in tumors. *Cancer Res.* **46,** 2821–2826
12. Bidani, A., Wang, C. Z., Saggi, S. J., and Heming, T. A. (1988) Evidence for pH sensitivity of tumor necrosis factor-α release by alveolar macrophages. *Lung* **176,** 111–121
13. Tannock, I. F., and Rotin, D. (1989) Acid pH in tumors and its potential for therapeutic exploitation. *Cancer Res.* **49,** 4373–4384
14. Grinstein, S., Swallow, C. J., and Rotstein, O. D. (1991) Regulation of cytoplasmic pH in phagocytic cell function and dysfunction. *Clin. Biochem.* **24,** 241–247
15. Kraus, M., and Wolf, B. (1996) Implications of acidic tumor microenvironment for neoplastic growth and cancer treatment: a computer analysis. *Tumor Biol.* **17,** 133–154
16. Saxena, H., Deshpande, D. A., Tiegs, B. C., Yan, H., Battafarano, R. J., Burrows, W. M., Damera, G., Panettieri, R. A., Dubose, T. D. Jr., An, S. S., and Penn, R. B. (2012) The GPCR OGR1 (GPR68) mediates diverse signaling and contraction of airway smooth muscle in response to small reductions in extracellular pH. *Br. J. Pharmacol.* **166,** 981–990
17. Wang, J. Q., Kon, J., Mogi, C., Tobo, M., Damirin, A., Sato, K., Komachi, M., Malchinkhuu, E., Murata, N., Kimura, T., Kuwabara, A., Wakamatsu, K., Koizumi, H., Uede, T., Tsujimoto, G., Kurose, H., Sato, T., Harada, A., Misawa, N., Tomura, H., and Okajima, F. (2004) TDAG8 is a proton-sensing and psychosine-sensitive G-protein-coupled receptor. *J. Biol. Chem.* **279,** 45626–45633

18. Ishii, S., Kihara, Y., and Shimizu, T. (2004) Identification of T cell death-associated gene8(TDAG8) as a novel acid sensing G protein-coupled receptor. *J. Biol. Chem.* **280,** 9083–9087
19. Radu, C. G., Nijagal, A., McLaughlin, J., and Wang, L., Witte, O. N. (2005) Differential proton sensitivity of related G protein-coupled receptors T cell death-associated gene 8 and G2A expressed in immune cells. *Proc. Natl. Acad. Sci. U. S. A.* **102,** 1632–1637
20. Choi, J. W., Lee, S. Y., and Choi, Y. (1996) Identification of a putative G protein-coupled receptor induced during activation-induced apoptosis of T cells. *Cell. Immunol.* **168,** 78–84
21. Weng, Z., Fluckiger, A. C., Nisitani, S., Wahl, M. I., Le, L. Q., Hunter, C. A., Fernal, A. A., Le Beau, M. M., and Witte, O. N. (2000) A DNA damage and stress inducible G protein-coupled receptor blocks cells in G2/M. *Proc. Natl. Acad. Sci. U. S. A.* **95,** 12334–12339
22. Xu, Y., Zhu, K., Hong, G., Wu, W., Baudhuin, L. M., Xiao, Y., and Damron, D. S. (2000) Sphingosylphosphorylcholine is a ligand for ovarian cancer G-protein-coupled receptor 1. *Nat. Cell Biol.* **2,** 261–267
23. Kabarowski, J. H. S., Feramisco, J. D., Le, L. Q., Gu, J. L., Luoh, S. W., Simon, M. I., and Witte, O. N. (2000) Direct genetic demonstration of Gα13 coupling to the orphan G protein-coupled receptor G2A leading to RhoA-dependent actin rearrangement. *Proc. Natl. Acad. Sci.* **97,** 12109–12114
24. Murakami, N., Yokomizo, T., Okuno, T., and Shimizu, T. (2004) G2A is a proton-sensing G-protein-coupled receptor antagonized by lysophosphatidylcholine. *J. Biol. Chem.* **279,** 42484–42491
25. Kabarowski, J. H., Zhu, K., Le, L. Q., Witte, O. N., and Xu, Y. (2001) Lysophosphatidylcholine as a ligand for the immunoregulatory receptor G2A. *Science* **293,** 702–705
26. Gräler, M. H., and Goetzl, E. J. (2002) Lysophospholipids and their G protein-coupled receptors in inflammation and immunity. *Biochim. Biophys. Acta* **1582,** 168–174
27. Ishii, I., Fukushima, N., Ye, X., and Chun, J. (2004) Lysophospholipid receptors: signaling and biology. *Annu. Rev. Biochem.* **73,** 321–354
28. Lin, P., and Ye, R. D. (2003) The lysophospholipid receptor G2A activates a specific combination of G proteins and promotes apoptosis. *J. Biol. Chem.* **278,** 14379–14386
29. Radu, C. G., Yang, L. V., Riedinger, M., Au, M., and Witte, O. N. (2004) T cell chemotaxis to lysophosphatidylcholine through the G2A receptor. *Proc. Natl. Acad. Sci. U. S. A.* **101,** 245–250
30. Reiter, E., and Lefkowitz, R. J. (2006) GRKs and beta-arrestins: roles in receptor silencing, trafficking and signaling. *Trends Endocrinol. Metab.* **17,** 159–165
31. Ferguson, S. S. G. (2001) Evolving concepts in G protein-coupled receptor endocytosis: the role in receptor desensitization and signaling. *Pharmacol. Rev.* **53,** 1–24
32. Von Zastrow, M. (2003) Mechanisms regulating membrane trafficking of G protein-coupled receptors in the endocytic pathway. *Life Sci.* **74,** 217–224
33. Milligan, G. (2003) Constitutive activity and inverse agonists of G protein-coupled receptors: a current perspective. *Mol. Pharmcol.* **64,** 1271–1276
34. Wang, L., Radu, C. G., Yang, L. V., Bentolila, L. A., Riedinger, M., and Witte, O. N. (2005) Lysophosphatidylcholine-induced surface redistribution regulates signaling of the murine G protein-coupled receptor G2A. *Mol. Biol. Cell* **16,** 2234–2247
35. Griffin, B. A., Adams, S. R., and Tsien, R. Y. (1998) Specific covalent labeling of recombinant protein molecules inside live cells. *Science* **281,** 269–272
36. Chen, I., Howarth, M., Lin, W., and Ting, A. Y. (2005) Site-specific labeling of cell surface proteins with biophysical probes using biotin ligase. *Nat. Methods* **2,** 99–104
37. Popp, M. W., Antos, J. M., Grotenbreg, G. M., Spooner, E., and Ploegh, H. (2007) Sortagging: a versatile method for protein labeling. *Nat. Chem. Biol.* **3,** 707–708
38. Tanaka, T., Yamamoto, T., Tsukiji, S., and Nagamune, T. (2008) Site-specific protein modification on living cells catalyzed by sortase. *Chembiochem* **9,** 802–807
39. Yamamoto, T., and Nagamune, T. (2009) Expansion of the sortase-mediated labeling method for site-specific N-terminal labeling of cell surface proteins on living cells. *Chem. Commun.* **9,** 1022–1024
40. Hirota, N., Yasuda, D., Hashidate, T., Yamamoto, T., Yamaguchi, S., and Nagamune, T., Nagase, T., Shimizu, T., and Nakamura, M. (2010) Amino acid residues critical for endoplasmic reticulum export and trafficking of platelet-activation factor receptor. *J. Biol. Chem.* **285,** 5931–5940
41. Matsumoto, T., Takase, R., Tanaka, T., Fukuda, H., and Kondo, A. (2012) Site-specific protein labeling with amine-containing molecules using Lactobacillus plantarum sortase. *Biotechnol. J.* **7,** 642–648
42. Ton-That, H., Liu, G., Mazmanian, S. K., Faull, K. F., and Schneewind, O. (1999) Purification and characterization of sortase, the transpeptidase that cleaves surface proteins of *Staphylococcus aureus* at the LPXTG motif. *Proc. Natl. Acad. Sci. U. S. A.* **96,** 12424–12429
43. Lippincott-Schwartz, J., and Patterson, G. H. (2003) Development and use of fluorescent protein markers in living cells. *Science* **300,** 87–90
44. Zhang, J., Campbell, R. E., Ting, A. Y., and Tsien, R. Y. (2002) Creating new fluorescent probes for cell biology. *Nat. Rev. Mol. Cell. Biol.* **3,** 906–918

*Received for publication March 11, 2014.*
*Accepted for publication May 12, 2014.*

Published OnlineFirst October 15, 2014; DOI: 10.1158/0008-5472.CAN-14-0643

Molecular and Cellular Pathobiology

Cancer Research

# Molecular Characterization of Chronic-type Adult T-cell Leukemia/Lymphoma

Noriaki Yoshida[1,2,3], Kennosuke Karube[1], Atae Utsunomiya[4], Kunihiro Tsukasaki[5], Yoshitaka Imaizumi[5], Naoya Taira[6], Naokuni Uike[7], Akira Umino[1,8], Kotaro Arita[1,9], Miyuki Suguro[1], Shinobu Tsuzuki[1], Tomohiro Kinoshita[10], Koichi Ohshima[3], and Masao Seto[1,2,3]

## Abstract

Adult T-cell leukemia/lymphoma (ATL) is a human T-cell leukemia virus type-1–induced neoplasm with four clinical subtypes: acute, lymphoma, chronic, and smoldering. Although the chronic type is regarded as indolent ATL, about half of the cases progress to acute-type ATL. The molecular pathogenesis of acute transformation in chronic-type ATL is only partially understood. In an effort to determine the molecular pathogeneses of ATL, and especially the molecular mechanism of acute transformation, oligo-array comparative genomic hybridization and comprehensive gene expression profiling were applied to 27 and 35 cases of chronic and acute type ATL, respectively. The genomic profile of the chronic type was nearly identical to that of acute-type ATL, although more genomic alterations characteristic of acute-type ATL were observed. Among the genomic alterations frequently observed in acute-type ATL, the loss of *CDKN2A*, which is involved in cell-cycle deregulation, was especially characteristic of acute-type ATL compared with chronic-type ATL. Furthermore, we found that genomic alteration of *CD58*, which is implicated in escape from the immunosurveillance mechanism, is more frequently observed in acute-type ATL than in the chronic-type. Interestingly, the chronic-type cases with cell-cycle deregulation and disruption of immunosurveillance mechanism were associated with earlier progression to acute-type ATL. These findings suggested that cell-cycle deregulation and the immune escape mechanism play important roles in acute transformation of the chronic type and indicated that these alterations are good predictive markers for chronic-type ATL. *Cancer Res; 74(21); 6129–38. ©2014 AACR.*

[1]Division of Molecular Medicine, Aichi Cancer Center Research Institute, Nagoya, Japan. [2]Department of Cancer Genetics, Nagoya University Graduate School of Medicine at Aichi Cancer Center Research Institute, Nagoya, Japan. [3]Department of Pathology, Kurume University School of Medicine, Kurume, Japan. [4]Department of Hematology, Imamura Bun-in Hospital, Kagoshima, Japan. [5]Department of Hematology, Atomic Bomb Disease and Hibakusha Medicine Unit, Atomic Bomb Disease Institute, Nagasaki University, Nagasaki, Japan. [6]Department of Internal Medicine, Heart Life Hospital, Nakagusukuson, Japan. [7]Department of Hematology, National Hospital Organization Kyushu Cancer Center, Fukuoka, Japan. [8]Hematology and Oncology, Mie University Graduate School of Medicine, Tsu, Japan. [9]Third Department of Internal Medicine, Graduate School of Medicine and Pharmaceutical Sciences, University of Toyama, Toyama, Japan. [10]Department of Hematology and Cell Therapy, Aichi Cancer Center, Nagoya, Japan.

**Note:** Supplementary data for this article are available at Cancer Research Online (http://cancerres.aacrjournals.org/).

Current address for N. Yoshida: Department of Pathology and Laboratory Medicine/Diagnostic Pathology, Nagoya University Graduate School of Medicine, Nagoya, Japan; current address for K. Karube: Hematopathology Section, Laboratory of Pathology, Hospital Clínic, Institut d'Investigacions Biomèdiques August Pi i Sunyer (IDIBAPS), University of Barcelona, Barcelona, Spain; and current address for K. Tsukasaki: Department of Hematology, National Cancer Center Hospital East, Kashiwa, Japan.

**Corresponding Author:** Masao Seto, Department of Pathology, Kurume University School of Medicine, 67 Asahimachi, Kurume, Fukuoka 830-0011, Japan. Phone: 81-942-35-3311, ext. 3181; 81-942-31-7547 (direct); Fax: 81-942-31-0342; E-mail: seto_masao@kurume-u.ac.jp and mseto@aichi-cc.jp

**doi:** 10.1158/0008-5472.CAN-14-0643



## Introduction

Adult T-cell leukemia/lymphoma (ATL) is a human T-cell leukemia virus type-1 (HTLV-1)–induced neoplasm (1, 2). Four clinical subtypes of ATL have been classified on the basis of clinical manifestation: acute, lymphoma, chronic, and smoldering (3). Among these subtypes, chronic-type ATL shows characteristic manifestations such as increased abnormal lymphocytes in peripheral blood, lactate dehydrogenase (LDH) levels up to twice the normal upper limit, and absence of hypercalcemia. Chronic-type ATL is relatively rare and its frequency is estimated to be 8% to 18% of ATL cases (3). Previous reports regard the chronic type as indolent ATL compared with acute/lymphoma types, which show an aggressive clinical course (3, 4). However, a recent study of indolent ATL demonstrated that about half of the patients with chronic-type ATL progress to acute-type ATL within approximately 18 months from diagnosis and subsequent death (4). This finding suggests that patients with chronic-type ATL also had a poor prognosis. High LDH, high blood urea nitrogen, and low albumin levels have been identified as poor prognostic factors for chronic-type ATL, and patients with chronic-type ATL with these poor prognostic factors therefore need to be treated by intensive chemotherapy as in the case of patients with aggressive ATL (5).

Disruptions of *CDKN2A*, *CDKN2B*, and *TP53* have been reported as candidate genes that play important roles in acute

Published OnlineFirst October 15, 2014; DOI: 10.1158/0008-5472.CAN-14-0643



transformation of chronic-type ATL (6–12). However, these acute transformation–related genetic alterations have been identified only by focusing on genes that were previously shown to be involved in tumor progression of other malignancies. Therefore, these genetic alterations may be indicative of acute transformation in some cases, although the molecular mechanism of acute transformation remains to be fully elucidated. Identification of the molecular characteristics of chronic-type ATL using unbiased and genome-wide methods can provide further insights to elucidate the acute transformation mechanisms in chronic-type ATL. However, the molecular pathogenesis of chronic-type ATL has long remained unknown due to its rarity (13).

In the present study, high-resolution oligo-array comparative genomic hybridization (aCGH) and gene expression profiling (GEP) were applied to 27 cases of chronic-type ATL in an effort to determine the molecular pathogenesis. The same approaches were used with 35 cases of acute-type ATL, and we then compared the molecular characteristics of chronic- and acute-type ATL to investigate the molecular mechanism of acute transformation.

## Materials and Methods

### Patient samples

We collected and analyzed 27 cases of chronic-type ATL and 35 cases of acute-type ATL (Table 1 and Supplementary Table S1 in Supplementary Data). These samples were obtained from patients at Imamura-Bunin Hospital (Kagoshima, Japan), Nagasaki University School of Medicine (Nagasaki, Japan), Heart Life Hospital (Nakagusukuson, Japan), and Kyushu Cancer Center (Fukuoka, Japan). In accordance with Shimoyama criteria, the diagnoses were made by expert hematologists (A. Utsunomiya, K. Tsukasaki, Y. Imaizumi, N. Taira, and N. Uike; ref. 3). Samples and medical records used in our study were approved by the Institute Review Board of the Aichi Cancer Center (Nagoya, Japan). Informed consent was obtained according to the Declaration of Helsinki from all patients. DNA and RNA used in this study were extracted from purified CD4-positive cells as previously reported (14). For the cumulative incidence of acute transformation, events were defined as acute transformation or any treatment for ATL.

### Copy number analysis by aCGH and GEP

We performed aCGH analysis on all samples using 400K aCGH (Agilent, Cat. # G4448A; Agilent Technologies) and 44K aCGH (Agilent, Cat. # G4413A) slides (Supplementary Table S1). Thirteen acute-type cases analyzed in a previous study were included (14). Procedures for DNA digestion, labeling, hybridization, scanning, and data analyses were performed according to the manufacturer's protocols (www.agilent.com). Raw data were transferred to the Genomic Workbench v5.0 software (Agilent Technologies) for further analysis as described previously (14–16). Among these identified alterations, we focused on minimal common regions (MCR). MCRs are defined as alterations that encompass less than 3 protein-coding genes among all samples analyzed in this study (17). Copy number variations/polymorphisms (CNV) were identified using a database (HS_hg18_CNV-20120403, Agilent), which was obtained from Database of Genomic Variants (http://projects.tcag.ca/variation/) in April 2012 and then excluded from further analyses as described previously (16). We also performed aCGH analysis on matched normal DNA samples that were available and confirmed that the identified MCRs were not CNVs (Supplementary Fig. S1A).

For analysis of GEP, the Whole Human Genome 44K Oligo-microarray Kit (Agilent, Cat. # G4112F) was used for the hybridization of labeled RNA. The total RNA of 13 chronic samples and 21 acute samples was analyzed. The experimental protocol used reflected the manufacturer's protocol (www.agilent.com) as previously reported (15, 16). Using the results of GEP, gene set enrichment analysis (GSEA) was performed as previously described (15, 16, 18).

The detailed description of these analyses can be found in Supplementary Methods. The microarray data were submitted to ArrayExpress and assigned accession numbers E-MTAB-1808 (aCGH) and E-MTAB-1798 (GEP).

### Mutation analyses of CD58 and β2-microglobulin

The exons 1–4 of *CD58* and 1 and 2 of *β2-microglobulin* (*B2M*), whose mutations were identified in peripheral T-cell lymphomas (PTCL; ref. 19), were amplified from gDNA using PCR. PCR primers used are detailed in the previous study (20). Twenty-six acute-type and 26 chronic-type ATL samples, for which adequate DNA was available, were analyzed. Direct sequencing of PCR products was performed through capillary electrophoresis using the ABI3100 sequencer (Applied Biosystems).

### Flow cytometry

Analysis of cell surface CD58 in ATL cell lines was performed using anti-CD58 PE antibody (AlCD58, Beckman Coulter).

**Table 1.** Patient information at sampling

| Subtype | No. of samples | Median age (range), y | Median WBC (range), u/L | Median LDH (range), IU/L | Median calcium (range), mg/dL | Median albumin (range), g/dL | Median BUN (range), mg/dL |
|---|---|---|---|---|---|---|---|
| Chronic type | 27 | 61 (42–81) | 1,1400 (6,000–22,100) | 233 (155–465) | 9.3 (8.4–10.2) | 4.2 (3.0–4.8) | 15.5 (7.4–26.4) |
| Acute type | 35 | 57 (32–85) | 2,1700 (4,100–224,800) | 688 (203–2,223) | 9.3 (7.7–17.4) | 3.8 (2.6–4.5) | NA |

Abbreviations: BUN, blood urea nitrogen; NA, not available; WBC, white blood cells.